A&A 552, A117 (2013)
DOI: 10.1051/0004-6361/201220826

Astronomy & Astrophysics

Mono-deuterated dimethyl ether: laboratory spectrum up to 1 THz

Torsion-rotational spectrum within the vibrational ground-state for the symmetric and asymmetric conformers and first detection in IRAS 16293-2422⋆

C. Richard[1], L. Margulès[1], E. Caux[2,3], C. Kahane[4], C. Ceccarelli[4], J.-C. Guillemin[5], R. A. Motiyenko[1], C. Vastel[2,3], and P. Groner[6]

[1] Laboratoire de Physique des Lasers, Atomes et Molécules, CNRS UMR 8523, Université Lille 1, 59655 Villeneuve d'Ascq Cedex, France
e-mail: cyril.richard@phlam.univ-lille1.fr, laurent.margules@univ-lille1.fr
[2] Université de Toulouse, UPS-OMP, IRAP, Toulouse, France
[3] CNRS, Institut pour la Recherche en Astrophysique et Planétologie, 9 Av. Colonel Roche, BP 44346, 31028 Toulouse Cedex 4, France
[4] UJF-Grenoble 1/CNRS-INSU, Institut de Planétologie et d'Astrophysique de Grenoble (IPAG) UMR 5274, 38041 Grenoble, France
[5] Institut des Sciences Chimiques de Rennes, UMR 6226 CNRS – ENSCR, Avenue du Général Leclerc, CS 50837, 35708 Rennes Cedex 7, France
[6] Department of Chemistry, University of Missouri-Kansas City, Kansas City, MO 64110-2499, USA

Received 30 November 2012 / Accepted 25 February 2013

ABSTRACT

Context. Dimethyl ether is one of the most abundant complex organic molecules (COMs) in star-forming regions. Like other COMs, its formation process is not yet clearly established, but the relative abundances of its deuterated isotopomers may provide crucial hints in studying its chemistry and tracing the source history. The mono-deuterated species (CH_2DOCH_3) is still a relatively light molecule compared to other COMs. Its spectrum is the most intense in the THz domain in the 100–150 K temperature regime, tracing the inner parts of the low-mass star-forming region. Therefore, it is necessary to measure and assign its transitions in this range in order to be able to compute accurate predictions required by astronomical observations, in particular with the telescope operating in the submm range, such as ALMA.
Aims. We present the analysis of mono-deuterated dimethyl ether in its ground-vibrational state, based on an effective Hamiltonian for an asymmetric rotor molecules with internal rotors. The analysis covers the frequency range 150–990 GHz.
Methods. The laboratory rotational spectrum of this species was measured with a submillimeter spectrometer (50–990 GHz) using solid-state sources. For the astronomical detection, we used the IRAM 30 m telescope to observe a total range of 27 GHz, in 4 frequency bands from 100 GHz to 219 GHz.
Results. New sets of spectroscopic parameters have been determined by a least squares fit with the ERHAM code for both conformers. These parameters have permitted the first identification in space of both mono-deuterated DME isomers via detection of twenty transitions in the solar-type protostar IRAS 16293-2422 with the IRAM 30 m telescope. The DME deuteration ratio in this source appears as high as observed for methanol and formaldehyde, two species known to play an important role in the COMs formation history.

Key words. line: identification – methods: laboratory – molecular data – techniques: spectroscopic – submillimeter: ISM – ISM: molecules

1. Introduction

Dimethyl ether (DME) is a large complex organic molecule (COM) detected for the first time in the interstellar medium (ISM) by Snyder et al. (1974). Abundant in the hot cores, which are the precursors of high-mass stars (Ikeda et al. 2001), DME is also one of the main COMs in hot corinos, forming low-mass stars, such as IRAS 16293-2422 (Cazaux et al. 2003; Bottinelli et al. 2004). In both types of sources, the commonly adopted scenario is that grain surface chemistry plays a crucial role in the formation of COMs in the early, cold prestellar stage of star formation; subsequently, during the warm up phase corresponding to the hot cores and hot corinos stages, the icy grain mantles evaporate and inject the products of grain surface chemistry into the molecular gas (Herbst & van Dishoeck 2009, and references therein). However, the relative importance of cold grain surface and post-evaporation warm gas-phase processes in the formation of DME is under debate (see e.g. Peeters et al. 2006; Brouillet et al. 2013). Furthermore, DME has been recently detected in a cold prestellar core, L1689B, (Bacmann et al. 2012), where the warm-up phase has not yet taken place. At least for DME, the COM formation scenario in protostars needs further investigations. Many hydrogenated molecules observed in hot corinos such as IRAS 16293-2422 show remarkably high D/H abundance ratios, significantly higher than observed in hot cores. This so-called super-deuteration phenomenon (Ceccarelli et al. 2007) is thought to be linked to molecular depletion on the grain

⋆ Full Tables A.1, A.2, B.1, and B.2, which respectively give the measured (in laboratory) and predicted frequencies, are only available at the CDS via anonymous ftp to cdsarc.u-strasbg.fr (130.79.128.5) or via http://cdsarc.u-strasbg.fr/viz-bin/qcat?J/A+A/552/A117

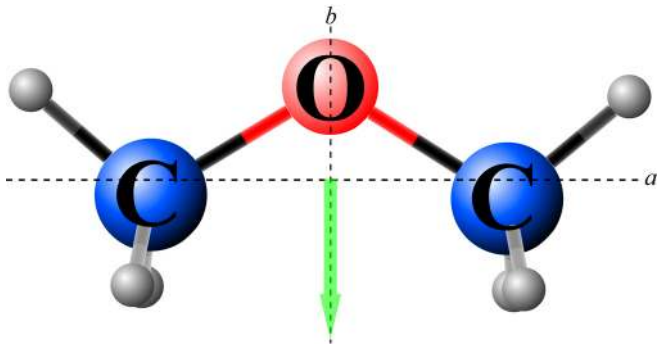

Fig. 1. Representation of the DME and of its electric dipole moment in the principal inertial axes. The dipole moment arrow is drawn from the negative to positive charge.

surface during the cold prestellar phase. However, deuterium chemistry in hot cores might be significantly different as shown by the distinct methanol deuterated species relative abundances (Ratajczak et al. 2011). Thus, measuring the deuteration ratio of DME in different types of sources is likely to provide constraints on this species chemistry and formation history. Even though dimethyl ether is such an abundant interstellar molecule, up to now, the mono-deuterated isotopologue has not been observed.

DME is a near-prolate asymmetric top ($\kappa = -0.922$ MHz) with only a b-dipole moment component, $\mu_b = 1.302$ D (Blukis et al. 1963). Figure 1 represents the molecule and its electronic dipole moment pointing from the negative to the positive poles along the b-axis. Previous laboratory investigations have been conducted for DME up to 2.1 THz (Groner et al. 1998; Endres et al. 2009). Upon partial deuteration on one of the methyl groups, the DME molecule can exist in one of two different conformations, each with a single CH_3 internal rotor. The symmetric conformation is characterized by the D atom located in the C-O-C plane, and thus by C_s symmetry. When the D atom is located outside of the C-O-C plane the corresponding conformation is called asymmetric. The asymmetric conformation has two equivalent configurations with a possible tunneling motion between them. In summary, one can expect to observe in the rotational spectrum of deuterated DME the typical A-E splittings due to the nonsubstituted methyl top internal rotation for both conformations, and additional doublet splitting of A and E lines of the asymmetric conformation due to tunneling of the CH_2D group.

The rotational spectrum of mono-deuterated DME in the vibrational ground-state (see simulated spectra at different temperatures in Fig. 2) was studied for the first time by Blukis et al. (1963). They measured a few transitions for several isotopic species in the centimeter-wave range (8.2–50 GHz) and determined the rotational constants. The starting point of our study was the analysis carried out in the same frequency range with better accuracy for almost all isotopic species by Niide & Hayashi (2003). In the present study, the set of assigned transitions was thus greatly extended to 1 THz, and data from this current investigation were combined with published data into a global fit for each conformer. At the same time, two new accurate sets of parameters were derived from the fits performed with the ERHAM code (Groner 1997, 2012). These new data are thus now precise enough to allow an astrophysical detection in the ISM.

This paper presents our laboratory investigation and analysis of mono-deuterated DME, as well as a detection in the solar-type protostar IRAS 16293-2422 using the IRAM 30 m telescope.

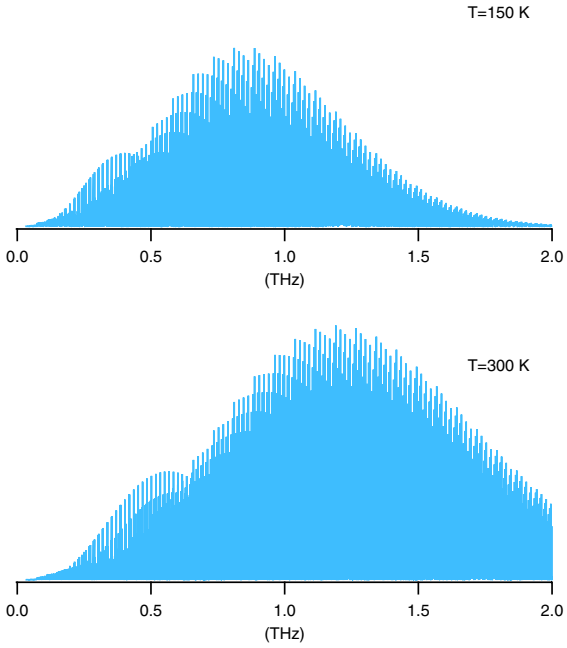

Fig. 2. Stick spectrum of mono-deuterated DME (symmetric conformer) in its vibrational ground state at 150 K (above) and 300 K (below). This figure illustrates the importance of the analysis around 1 THz. Although the dense ISM is generally colder, such temperatures exist in the warm inner regions of the collapsing protostars (see for instance Ceccarelli et al. 2000). The spectrum intensity scale is arbitrary.

2. Experimental details

2.1. Preparation of mono-deuterated dimethyl ether

The synthesis of mono-deuterated DME has already been reported by Shtarev et al. (1999) and has been modified as follows. Lithium aluminum deuteride (420 mg, 10 mol) and tetraglyme (20 mL) were introduced into a 100 mL two-necked flask equipped with a stirring bar, a stopcock, and a septum. The flask was fitted to a vacuum line equipped with two traps. The flask was immersed in a cold bath (−25 °C) and degassed. The stopcock was then closed. Bromomethyl methyl ether (2.5 g, 20 mmol) diluted in tetraglyme (5 mL) was added slowly with a syringe through the septum. At the end of the addition, the mixture was stirred for 30 min at room temperature. The first trap was then immersed in a −80 °C cold bath and the second one in a liquid nitrogen bath (−196 °C). The stopcock of the cell was opened slowly. Residual bromomethyl methyl ether and high boiling impurities were condensed in the first trap, and mono-deuterated DME was selectively condensed in the second trap. The yield was 80% based on the starting brominated ether.

2.2. Lille – submillimeter wave spectrometer

The submillimeter-wave measurements were performed with the Lille spectrometer (150–990 GHz) (Motiyenko et al. 2010). The sources are only solid-state devices. The frequency of the Agilent synthesizer (12.5–17.5 GHz) was first multiplied by six and amplified by a Spacek active sextupler providing the output power of +15 dBm in the W-band range (75–110 GHz). This power is high enough to use passive Schottky multipliers (×2, ×3, ×5, ×2×3, ×3×3) from Virginia Diodes Inc. in the next stage of the frequency multiplication chain. As a detector we used an InSb liquid He-cooled bolometer from QMC Instruments Ltd. to improve the sensitivity of the spectrometer; the source

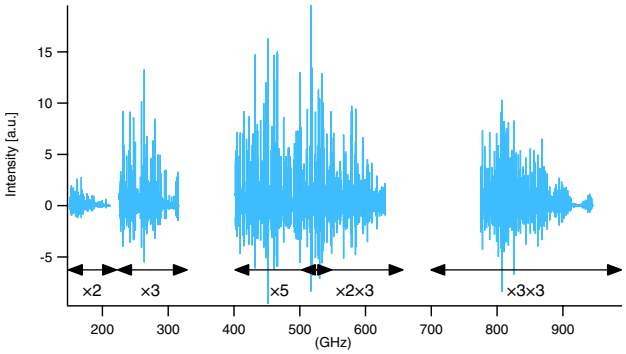

Fig. 3. Spectrum of mono-deuterated DME recorded at Lille is represented with each multiplier range (×2, ×3, ×5, ×2×3, ×3×3), which cover most of the frequencies up to 990 GHz. The spectrum intensity scale is arbitrary.

was frequency-modulated at 10 kHz. The absorption cell was a stainless-steel tube (6 cm diameter, 220 cm long). The sample pressure during measurements was about 1.5 Pa (15 μbar), and the linewidth was limited by Doppler broadening. These measurements were performed at room temperature. The measurement accuracy for isolated lines is estimated to be better than 30 kHz up to 630 GHz and 50 kHz at higher frequencies owing to the Doppler effect. However, if the lines were blended or had a poor signal-to-noise ratio, they were assigned an uncertainty of 100 or even 200 kHz. The spectrum of mono-deuterated DME recorded at Lille appears in its entirety in Fig. 3.

3. Spectral analysis

This analysis of the spectrum of mono-deuterated DME was undertaken to extend the work of Niide & Hayashi (2003). Previous parameters and assigned transitions were used for the initial prediction with the ERHAM code (Groner 1997, 2012) in Watson's A reduction (Watson 1977). Then, the prediction was improved step by step with the addition of new identified lines. The XIAM program (Hartwig & Dreizler 1996) was also used for comparisons, but owing limitations in the program for blended transitions, fits results were poorer so are not presented in this paper except for the barrier height for rotation of the methyl group, V_3.

Mono-deuterated DME shows a very complex spectrum, and there are a lot of unassigned lines due to the excited torsional states about 200–240 cm^{-1} above the ground state (values given by Endres et al. (2010) for the parent species). In addition, many lines are blended or distorted. As a rule, lines with residuals higher than 4σ were excluded from the fit. Since the principal axes in mono-deuterated DME have almost the same orientation with respect to the molecular frame as in normal DME, the dipole moment in mono-deuterated DME is almost parallel to the b axis; in consequence, the spectrum contains mainly b-transitions. However, Groner et al. (1998) report that "forbidden" c-transitions can occur when pseudo-quantum numbers K_a and K_c do not represent the wave functions very well in the case of mixing or level crossing. In our analysis, a few c-transitions have been assigned especially at high frequency. Transitions without intense torsional-rotational interaction obey b-type asymmetric top selection rules: $\Delta J = 0, \pm 1; \Delta K_a = \pm 1, 3, \ldots; \Delta K_c = \pm 1, 3, \ldots$ (Gordy & Cook 1984). The spin weight for both substates A and E is 4. The spectroscopic parameters and their uncertainties are presented in Table 1 for both conformers.

Table 1. Spectroscopic constants of the ground-vibrational state of mono-deuterated DME for the two different conformers.

Parameters	Symmetric conformer	Asymmetric conformer
ρ	0.216545(71)	0.19175(13)
β (deg)	7.545(9)	9.718(24)
α (deg)	0.0[a]	0.0[b]
A (MHz)	38 281.53382(35)	34 764.30530(33)
B (MHz)	9309.18796(13)	9642.41649(12)
C (MHz)	8277.96648(11)	8537.25156(12)
Δ_J (kHz)	7.06511(11)	8.97763(10)
Δ_{JK} (kHz)	−20.32475(64)	−18.29447(56)
Δ_K (kHz)	297.4899(30)	245.4877(22)
δ_J (kHz)	1.281232(37)	1.835770(33)
δ_K (kHz)	−8.9793(21)	−9.3752(32)
Φ_J (Hz)	0.004839(35)	0.006426(25)
Φ_{JK} (Hz)	0.0925(23)	0.1800(22)
Φ_{KJ} (Hz)	−3.2546(79)	−3.5559(73)
Φ_K (Hz)	10.078(11)	9.5379(70)
ϕ_J (Hz)	0.002403(15)	0.003130(11)
ϕ_{JK} (Hz)	0.1716(15)	0.2760(11)
ϕ_K (Hz)	1.649(89)	4.446(71)
ϵ_1 (MHz)	−2.9882(33)	−2.5032(60)
$[A-(B+C)/2]_1$ (kHz)	0.951(42)	0.663(55)
$[(B+C)/2]_1$ (kHz)		−0.0281(79)
$[(B-C)/4]_1$ (kHz)	0.1349(33)	0.1140(46)
V_3[c] (cm^{-1})	906.61(75)	905.84(121)
Lines[d]	1253	1286
J(max), K_a(max)	54, 15	55, 19
L_{worst}[e]	3.5	−3.8
n[f]	20	21
σ_{fit}[g] (MHz)	0.091	0.104
σ_w[h]	1.06	1.12

Notes. Numbers in parentheses are one standard deviation in the same units as the last digit. [(a)] By symmetry. [(b)] Assumed, see Sect. 4. [(c)] Barrier height for rotation of the methyl group determined with XIAM. This parameter is not considered in the ERHAM fit. [(d)] Number of distinct lines in the fit. [(e)] ($o.-c.$)/error of the poorest-fit line. [(f)] Number of free parameters used in the fit. [(g)] Standard deviation of the fit. [(h)] Weighted standard deviation (dimensionless).

For the symmetric conformer, the fit includes 1255 distinct lines (1219 new lines). The lines were fitted with J up to 54 and K_a up to 15. A total of 20 spectroscopic parameters were determined by the least-squares method and are listed in Table 1. The fifteen nontunneling parameters correspond to the rotational and distortion constants. In addition, two internal rotation parameters (ρ and β), one energy tunneling parameter (ϵ_1) and two rotational constant tunneling parameters ($[A-(B+C)/2]_1$ and $[(B-C)/4]_1$) were determined. The notation used in this paper was developed in detail by Groner (1997). The weighted (dimensionless) standard deviation of the fit is of 1.06, while the rms (for the unweighted frequencies) is of 91 kHz.

Then, 1286 distinct lines (1251 new lines) were assigned and included in the fit for the asymmetric conformer. Three lines from the previous study (Niide & Hayashi 2003) were removed from the final fit because of higher residuals (more than 4σ). In addition, three other microwave lines originally assigned to the A state by Niide & Hayashi (2003) were attributed to the E state, and another tunneling coefficient was determined ($[(B+C)/2]_1$). The total of the transitions was fitted with $0 \leq J \leq 55$ and a K_a value up to 19. Table 1 presents the 21 parameters determined. The fit gives a weighted standard deviation of 1.12 and an rms of 104 kHz.

4. Discussion

The ground-vibrational state rotational spectrum of mono-deuterated DME (CH_2DOCH_3) was measured and analyzed in the frequency range up to 1 THz for both conformers. All experimental frequencies given in Tables A.1 and A.2 are available in their entirety in electronic form at the CDS. Only 17 and 19 frequencies for the symmetric and asymmetric conformers, respectively, deviated by more than 3σ. In both cases, lines with residuals greater than 4σ were assigned but not included in the fit, and these frequencies are reported in Tables A.1 and A.2 with an uncertainty of 0.

It seems that somewhat better results were obtained for symmetric conformer in the least-squares fit. Indeed, in the case of asymmetric conformer, tunneling between two equivalent configurations leads to Coriolis-type perturbations in the spectra that cannot be accounted for in the present ERHAM code. Moreover, some series of A and E lines of asymmetric conformer exhibit additional doublet structure due to the tunneling. This effect was particularly visible within the first members of Q branches and at low frequency, i.e., for the lines with low K_a ($\leq$5) and J ($\leq$15). Indeed, the splitting increases as J decreases as shown in Fig. 4. Another example of the quartets for R lines is given in Fig. 5. In all these cases, the center frequency of the doublet was entered as the transition frequency in the ERHAM fit, and an uncertainty of 0.1 MHz was assumed. This method has been used for 89 lines between 150 and 290 GHz. Fortunately for the present investigation, most of the lines showed doublets (twice as intense as for the symmetric conformer); therefore, it was possible to use the one-top approximation for the CH_3 group as long as no quartets were included in the fit. The correct treatment of such additional doubling requires inclusion of new Coriolis-type terms in the model.

Unlike the symmetric conformation, the asymmetric conformer does not have a symmetry plane. Therefore at the beginning, α, the angle of the ρ axis with regard to ab principal plane, was set to an arbitrary value of 10°. The subsequent least-squares fit resulted in an extremely low value for α, much less than 1°. As a consequence, α was set to zero for the final fit.

Another interesting quantity reported in Table 1 is the barrier height V_3, which was derived with the XIAM code and, therefore, not used in the fit of the free spectroscopic parameters listed in the table. Its value, either for the symmetric or the asymmetric configuration, is in good agreement with earlier work (Durig et al. 1976; Lovas et al. 1979) for the parent species.

5. Prediction

The newly derived sets of spectroscopic constants shown in Table 1 have permitted predictions of transition frequencies for the symmetric and asymmetric conformers up to 1.2 THz.

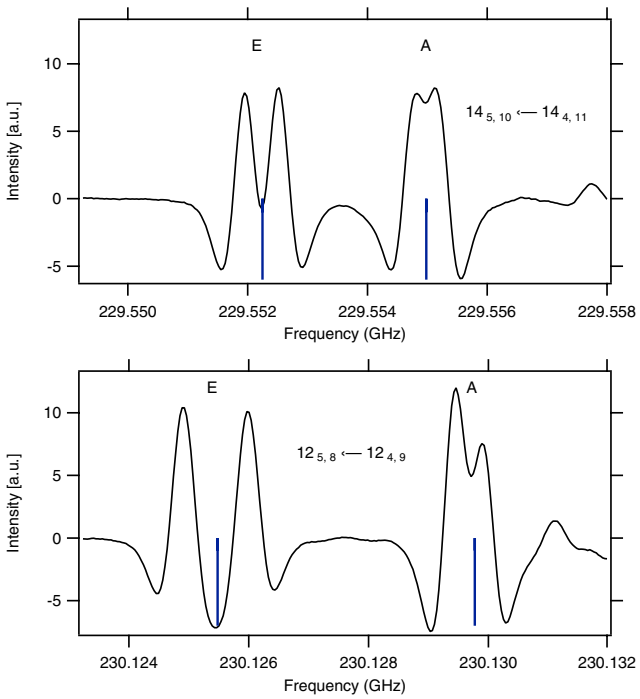

Fig. 4. Rotational transitions $J_{K_a,K_c} = 14_{5,10} \leftarrow 14_{4,11}$ and $J_{K_a,K_c} = 12_{5,8} \leftarrow 12_{4,9}$ of asymmetric mono-deuterated DME in the vibrational ground state at 230 GHz. Stick spectrum below experimental lines represents the prediction given by ERHAM. The internal motion of the CH_2D group is observed through the A and E components, which are split into two substates. It is also noticeable that this separation increases as J decreases and it is more intense in the E component. The experimental measurements are peaked in the center of the doublet. The spectrum intensity scale is arbitrary.

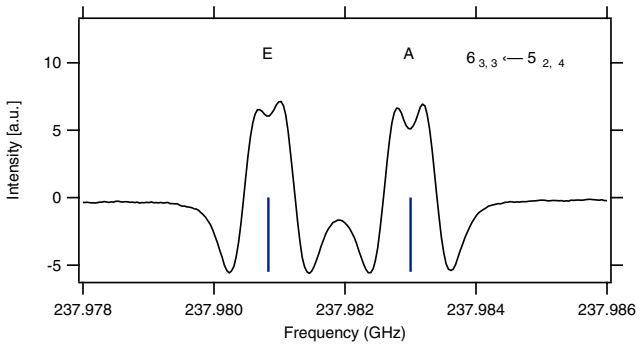

Fig. 5. Rotational transition $J_{K_a,K_c} = 6_{3,3} \leftarrow 5_{2,4}$ of asymmetric mono-deuterated DME in the vibrational ground state at 238 GHz. In the case of an R line, the splitting of the A and E states is nearly identical unlike in the Q line as represented in Fig. 4. The spectrum intensity scale is arbitrary.

Two short examples are provided in Tables B.1 and B.2 from 301.6 GHz to 303.5 GHz. The complete tables are available through the CDS. Calculated frequencies for both torsional substates A and E (symmetry numbers 0 and 1, respectively) are given with their line strength S for the μ_b component. To obtain the proper transition intensity, S must be multiplied by the square of μ_b and by the spin weight. Lines with $S < 0.1$, uncertainty $\geq$0.2 MHz, and $J > 60$ were removed from the predictions in order to keep only those lines that could be relevant for an astrophysical detection. In addition, a modified version of ERHAM provided predictions in the format of the JPL catalog (Pickett 1991).

Table 2. Rotational partition function for the symmetric and asymmetric conformers of mono-deuterated DME in the ground vibrational state computed for nine different temperatures.

Temperature	2.275 K	5 K	9.375 K	18.75 K	37.5 K	75 K	150 K	225 K	300 K
					Symmetric conformer				
A state	58.6	142.5	361.4	1015.2	2861.7	8082.2	22 850.4	41 941.2	64 256.6
E state	58.6	142.5	361.4	1015.2	2861.7	8082.2	22 850.4	41 941.2	64 256.6
Total	**117.2**	**285.0**	**722.8**	**2030.4**	**5723.5**	**16 164.3**	**45 700.8**[a]	83 882.3[b]	128 513.1[b]
Approx.[c]	111.7	277.6	712.8	2016.0	5702.2	16 164.3	45 617.5	**83 804.6**	**129 025.6**
Ratio	1.049	1.027	1.014	1.007	1.004	1.002	1.002	1.001	0.996
					Asymmetric conformer				
A state	119.2	289.6	734.2	2061.8	5811.8	16 413.5	46 407.7	85 201.7	130 629.7
E state	119.1	289.5	734.1	2061.8	5811.8	16 413.5	46 407.7	85 201.7	130 629.7
Total	**238.3**	**579.1**	**1468.3**	**4123.7**	**11 623.5**	**32 826.9**	**92 815.4**[a]	170 403.4[b]	261 259.3[b]
Approx.[c]	226.8	563.7	1447.4	4093.7	11 578.8	32 749.9	92 630.6	**170 173.4**	**261 999.0**
Ratio	1.051	1.027	1.014	1.007	1.004	1.002	1.002	1.001	0.997

Notes. The data presented in bold are the results used for the astrophysical detection in Sect. 7. This table is given for the rotational degrees of freedom; the contributions from vibrational excited states are ignored. [(a)] The sum of states did not converge completely, error for total <20 for the symmetric conformation, <40 for asymmetric. [(b)] The sum of states has not converged (this is the reason for ratio <1 at 300 K). [(c)] These values are computed with the rigid asymmetric rotor approximation.

Numerical values of the overall partition function were computed for nine different temperatures and listed in Table 2 in order to derive column densities. The results for the asymmetric conformation are multiplied by two because of the additional degeneracy discussed in Sect. 4. However, the intensity calculation in ERHAM for the JPL catalog format file does not consider this additional degeneracy. To arrive at the proper overall intensity for the asymmetric conformer, one needs to multiply the catalog intensity by two or divide the quoted sum of states by two.

6. Observations

We have successfully searched for the deuterated DME lines in the nearby low-mass protostar IRAS 16293-2422 (hereinafter IRAS 16293). Located in the Ophiuchi complex at 120 pc from the Sun (Loinard et al. 2008), IRAS 16293 has played a similar role to a prototype for low-mass protostars in astrochemical studies, such as Sgr B2 or Orion KL for high-mass protostars. Many complex organic molecules (COMs) have been detected towards IRAS 16293 including DME (Cazaux et al. 2003; Caux et al. 2011), with abundances comparable to those found in high-mass protostars. Because the level of molecular deuteration is considerably higher in low-mass protostars than in their massive counterparts (Ceccarelli et al. 2007), IRAS 16293 is thus the best candidate to look for deuterated DME. The data presented here come from recent observations, performed in March 2012 in four selected frequency ranges at 3, 2, and 1 mm, with the new broad band EMIR receivers at the IRAM 30 m telescope. IRAS 16293 hosts in a common colder envelope, two hot corinos, A (southeast) and B (northwest), separated by about 4″ (Wooten 1989).

Our observations, performed in DBS (double-beam-switch) observing mode with a 90″ throw, were centered on the B component at $\alpha(2000.0) = 16^{\rm h}32^{\rm m}22.6^{\rm s}$, $\delta(2000.0) = -24°28'33''$. The pointing and focus were checked every two hours on nearby planets or on continuum radio sources (1741-038 or 1730-130). The pointing accuracy was better than 2″, and even at the highest frequencies, the A and B components were both inside the beam of our observations so that the observed emission includes the contributions from both cores. Interferometric observations show that the molecular lines emitted by core B are much narrower than those emitted by core A (Bottinelli et al. 2004) and that DME lines emitted by core B are at least as strong as DME lines emitted by core A (Jørgensen et al. 2011). The TIMASSS survey (The IRAS 16293-2422 Millimeter And Submillimeter Spectral Survey, Caux et al. 2011) performed with the IRAM 30 m telescope and JCMT telescopes confirms that narrow DME lines from B are easily detected when contributions from both sources are simultaneously observed. This represents an additional favorable factor for identifying of deuterated DME lines in the spectrum from IRAS 16293, since it reduces the risk of blending by nearby lines from other species.

Table 3. Observational parameters.

Frequency (GHz)	HPBW (″)	Spectral resolution (MHz)	RMS (mK)
100.5–109.8	23	0.195	3–4.8
146.7–150.8	16	0.195	7.1–9.1
165.7–169.8	14	0.195	18.7–22.7
209.5–218.8	12	0.195	15.2–19.7

Comparison of the line intensities with those of the TIMASSS survey (Caux et al. 2011) shows that the calibration is accurate within 15%. Table 3 summarizes the observed bands and the details of the observations. Several representative spectra are plotted in Fig. 6.

7. Results: mono-deuterated DME identification in IRAS 16293

Thanks to the spectral resolution and the sensitivity of our IRAM 30 m observations, we were able to identify the 20 brightest lines of both forms of mono-deuterated DME, eight lines for the symmetric conformer and 12 lines for the asymmetric one (see Table 4) in the 27 GHz wide frequency range covered by our spectra. As for most complex molecules, mono-deuterated DME shows a very large number of transitions between 100 GHz and 220 GHz, and many of them were expected to be very faint. The identification was therefore checked using thresholds on both the upper energy level of the lines, restricted to $E'_{\rm max} \leq 100$ K and their Einstein coefficient, restricted to $A_{ij} \geq 10^{-5}$.

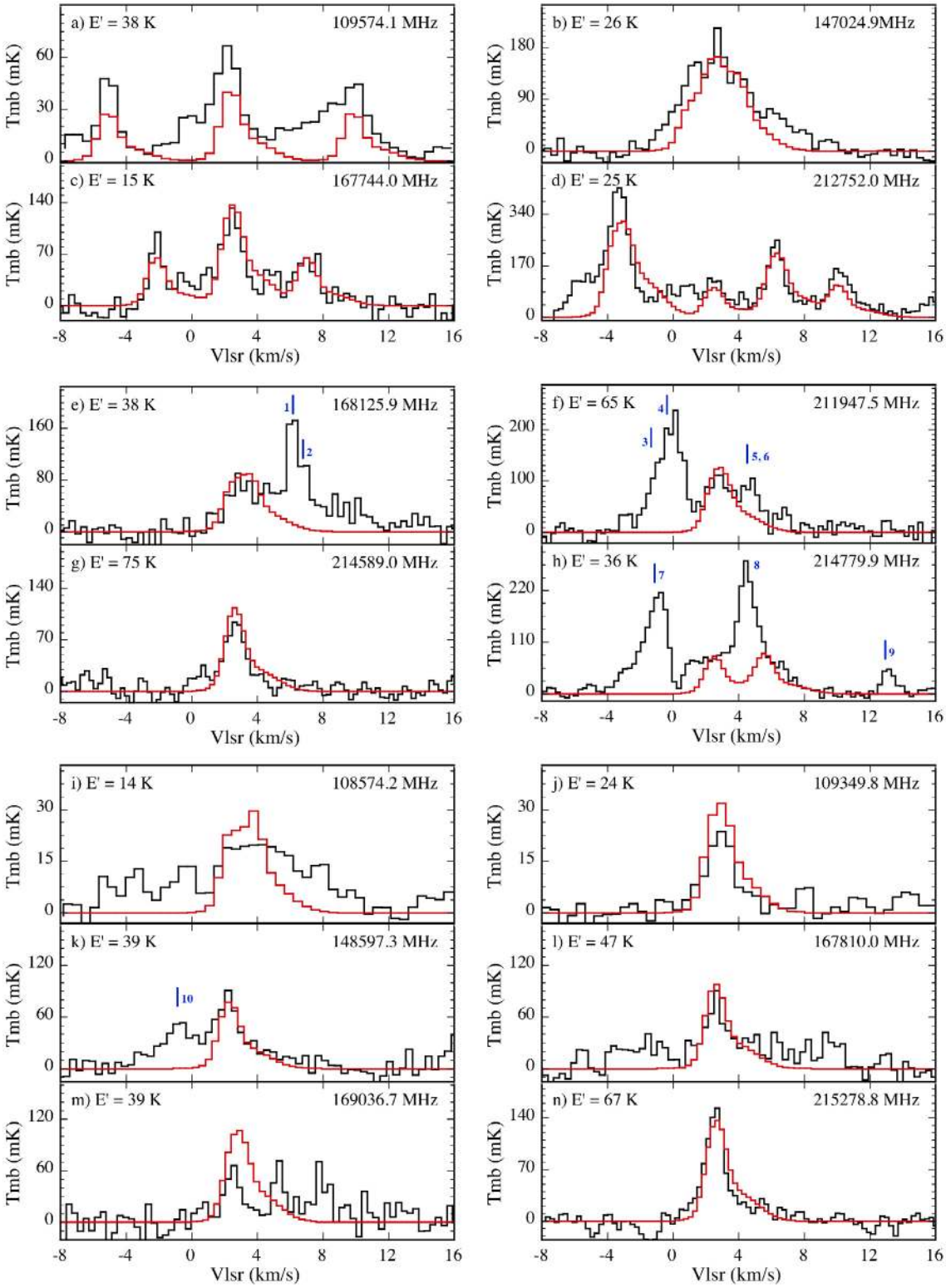

Fig. 6. Some observed transitions of DME and DME-1D (black) and the computed LTE model (red) using the CASSIS software. *E* values are the upper energy level of the observed lines. The notation *E* refers to the notation used in Table 1. The LTE model has been computed in bins of the same spectral resolution as the observations. Other transitions from other species are also present in these spectra. Panels **a)** to **d)**: some observed transitions of DME. Panels **e)** to **h)**: all detected transitions of DME-1D-sym. Panel **e)** DME-1D-sym ($9_{1,9}-8_{0,8}$) *E* and *A* lines. The blended lines are 1: $OC^{33}S$ (14−13) and 2: C_2H_5OH (10−9). Panel **f)** DME-1D-sym ($12_{1,12}-11_{0,11}$) *E* and *A* lines. The blended lines are 3: $HCOOCH_3$ (17−16) and 4, 5, 6: CH_3CHO (11−10) transitions. Panel **g)** DME-1D-sym ($13_{1,13}-12_{1,12}$) *E* and *A* lines. Panel **h)** DME-1D-sym ($8_{2,7}-7_{1,6}$) *E* and *A* lines. The blended lines are 7: $HCOOCH_3$ (18−17), 8: $H_2C^{18}O$ ($3_{1,2}-2_{1,1}$) and one unidentified line (9: around 13 km s^{-1}). Panels **i)** to **n)**: All detected transitions of DME-1D-asym. Panel **i)** DME-1D-asym ($5_{1,5}-4_{0,4}$) *E* and *A* lines. Panel **j)** DME-1D-asym ($7_{0,7}-6_{1,6}$) *E* and *A* lines. Panel **k)** DME-1D-asym ($9_{0,9}-8_{1,8}$) *E* and *A* lines. The blended line is 10: $HC(O)NH_2$ ($7_{4,4}-6_{4,3}$). Panel **l)** DME-1D-asym ($10_{0,10}-9_{1,9}$) *E* and *A* lines. Panel **m)** DME-1D-asym ($9_{1,9}-8_{0,8}$) *E* and *A* lines. Panel **n)** DME-1D-asym ($12_{1,12}-11_{0,11}$) *E* and *A* lines.

Table 4. Mono-deuterated DME observed lines for both conformations.

$N^{(a)}$	$\sigma^{(b)}$	J'	K'_a	K'_c	J''	K''_a	K''_c	Frequency (MHz)	E' (K)	A_{ij} (s^{-1})	rms (mK)	δV (km s^{-1})	ΔV (km s^{-1})	$T_{mb}\Delta V$ (mK km s^{-1}) obs.	mod.	5σ	Detected
Symmetric conformer																	
1	1	7	0	7	6	1	6	101 503.8	23	2.83×10^{-5}	5.6	0.55	[−2, 8]	30	64	65	no
2	0	7	0	7	6	1	6	101 503.2									
3	1	7	2	6	7	1	7	103 200.3	29	2.43×10^{-5}	3.7	0.55	[0, 7]	0	24	36	no
4	0	7	2	6	7	1	7	103 197.7	29	2.43×10^{-5}	3.7	0.55	[0, 7]	2	24	36	no
5	1	14	1	13	14	0	14	107 329.6	92	2.03×10^{-5}	3.7	0.55	[0, 7]	0	5	36	no
6	0	14	1	13	14	0	14	107 331.6	92	2.03×10^{-5}	3.7	0.55	[0, 7]	12	5	36	no
7	1	8	2	7	8	1	8	107 480.9	36	2.62×10^{-5}	3.6	0.55	[0, 7]	31	23	35	no
8	0	8	2	7	8	1	8	107 478.3	36	2.62×10^{-5}	3.6	0.55	[0, 7]	19	23	35	no
9	1	9	1	9	8	0	8	168 125.3	38	1.52×10^{-4}	14.2	0.35	[0, 6]	269	254	61	yes[e]
10	0	9	1	9	8	0	8	168 125.9									
11	1	12	1	12	11	0	11	211 947.1	65	3.05×10^{-4}	13.4	0.27	[1, 7]	397	283	85	yes[f]
12	0	12	1	12	11	0	11	211 947.5									
13	1	13	0	13	12	1	12	214 588.8	75	3.16×10^{-4}	8.4	0.27	[0, 8]	224	226	62	yes[g]
14	0	13	0	13	12	1	12	214 589.0									
15	1	8	2	7	7	1	6	214 777.7	36	1.77×10^{-4}	11.1	0.27	[1, 4]	200	180	50	yes[h]
16	0	8	2	7	7	1	6	214 779.9	36	1.77×10^{-4}	11.1	0.27	[1, 4]	412	180	50	yes[h]
Asymmetric conformer																	
17	1	9	2	8	9	1	9	102 689.8	44	1.04×10^{-5}	4.0	0.55	[0, 6]	35	18	36	no
18	0	9	2	8	9	1	9	102 691.7	44	1.04×10^{-5}	4.0	0.55	[0, 6]	26	18	36	no
19	1	10	0	10	9	1	9	108 481.1	53	1.14×10^{-5}	4.0	0.55	[0, 6]	24	17	36	no
20	0	10	0	10	9	1	9	108 483.0	53	1.14×10^{-5}	4.0	0.55	[0, 6]	12	17	36	no
21	1	5	1	5	4	0	4	108 573.7	14	1.99×10^{-5}	3.7	0.55	[0, 8]	100	103	58	yes[i]
22	0	5	1	5	4	0	4	108 574.2									
23	1	7	0	7	6	1	6	109 349.5	24	1.85×10^{-5}	3.7	0.55	[0, 8]	51	93	39	yes[j]
24	0	7	0	7	6	1	6	109 349.8									
25	1	9	0	9	8	1	8	148 597.1	39	5.13×10^{-5}	7.2	0.40	[1, 8]	214	192	60	yes[k]
26	0	9	0	9	8	1	8	148 597.3									
27	1	10	0	10	9	1	9	167 809.8	47	7.61×10^{-5}	14.4	0.35	[0, 6]	153	237	104	yes[l]
28	0	10	0	10	9	1	9	167 810.0									
29	1	9	1	9	8	0	8	169 036.3	39	7.94×10^{-5}	14.7	0.35	[0, 8]	228	288	123	yes[m]
30	0	9	1	9	8	0	8	169 036.7									
31	1	12	1	12	11	0	11	215 278.6	67	1.67×10^{-4}	10.2	0.27	[0, 8]	297	328	75	yes[n]
32	0	12	1	12	11	0	11	215 278.8									

Notes. Parameters of the mono-deuterated DME observed lines: δV is the spectral resolution, ΔV is the velocity interval on which the intensities have been integrated for each line. It varies with the frequency and is tuned to minimize the contribution of blending lines from other species (see Fig. 6). The columns "$T_{mb}\Delta V$" give the integrated intensities over these ΔV intervals for the observations (obs.), for the model (mod.) and for the 5σ (5σ) detection limit in these intervals (1σ = rms × $\sqrt{\delta V \times \Delta V}$). Lines for which the integrated intensity is greater than 5σ are considered as detected and are presented in Fig. 6 (the [i] in the column "detected" refers to Fig. 6 panels). For lines too close in frequency to be separated, the integrated intensities is given for both lines merged. [a] Numbering of the transitions; [b] symmetry number: 0(A), 1(E).

The lines listed in Table 4 are detected with an S/N higher than 5 (see Fig. 6). Other rotational transitions from both forms of mono-deuterated DME lie in the observed frequency range. According to the predictions of the LTE (local thermodynamic equilibrium) model based on the detected lines (see below), the intensities of these transitions are weak, and their non-detection is coherent with the noise of our observations.

In the same frequency range, several transitions of the main DME isotopomer are present as well (see Fig. 6). To derive the DME main and deuterated isotopomers column densities, we have assumed that emission from all three species were in LTE.

As mentioned above, both source A and source B contribute to the observed emission. The ALMA interferometric observations obtained during the Science Verification program, allow the central velocity V_{lsr} and the linewidth FWHM of each contribution to be estimated precisely (Pineda et al. 2012), and we used these values as fixed parameters in our LTE modeling of the DME lines.

In contrast, the source sizes, as determined by the interferometric observations, cannot directly be used to model single-dish observations because a fraction of the extended emission collected in the single-dish spectra is partly lost in the interferometric observations. We therefore adjusted the size of the two components in the LTE modeling, and we estimate that the uncertainties on the sizes of the two components adjusted in the LTE modeling are ~50% so that it introduces an uncertainty

Table 5. Physical parameters of the DME species adopted and derived from the LTE modeling.

Core	V_{lsr} (km s^{-1})	*FHWM* (km s^{-1})	Size ($''$)	T_{rot} (K)	N^a (10^{15} cm^{-2})	$N_a{}^b$ (10^{14} cm^{-2})	$N_s{}^c$ (10^{14} cm^{-2})	D/H (%)
A	3.8	3.0	1.2	30(±10)	5.0(±2)	2.5	5.0	~15
B	2.6	1.2	2.0	30(±10)	20.0(±5)	10.0	20.0	~15

Notes. This model is displayed in Fig. 6. The values in parenthesis are 1σ uncertainties. $^{(a)}$ Column density of DME. $^{(b)}$ Column density of symmetric conformation of mono-deuterated DME. $^{(c)}$ Column density of asymmetric conformation of mono-deuterated DME.

of about a factor 2 on the derived column densities. In the following, we used the CASSIS software[1] and computed synthetic spectra over a large grid of column densities and rotation temperatures [N, T_{rot}] for each of the two cores assuming LTE[2]. We then performed a χ^2 minimization of the model line profiles using the corresponding [N, T_{rot}] values, compared to the observed lines, as

$$\chi^2 = \sum_{i=1}^{n_{lin}} \sum_{j=1}^{n_{chan}} \frac{(I_{obs,ij} - I_{mod,ij})^2}{(rms_i)^2}, \quad (1)$$

where n_{lin} is the number of lines i, n_{chan} the number of channels j for each line, $I_{obs,ij}$ and $I_{mod,ij}$ the intensities observed and predicted by the model respectively in the channel j of the line i, and rms_i the rms of the line i (Coutens 2012). This minimization therefore gives the best-fit column densities and rotational temperature, as well as their corresponding uncertainties, which best reproduce our observations of DME. These values are listed in Table 5.

For the mono-deuterated DME species, we assumed, for each core, the same linewidth, central velocity, source size, and rotation temperature as for the main DME species and we have only adjusted the column densities to obtain the best fit to the observed lines. The resulting column densities are listed in Table 5.

The asymmetric conformation of mono-deuterated DME appears to be two times more abundant than the symmetric conformation of mono-deuterated DME on both sources. This result is simply the consequence of the statistical redistribution of D atoms due to a substitution of an H atom by a D atom in the main DME isotopomer. The total DME deuteration ratio is given by the fraction $[N_a + N_s]/N$. It is ~15% for both A and B components, so much higher than the cosmic D/H value of 1.5×10^{-5} (Linsky 2003) and comparable to "super-deuteration" ratios measured in IRAS 16293 for H_2CO and CH_3OH (Loinard et al. 2000; Parise et al. 2002). This result represents a strong constraint for the chemical modeling of the DME formation and deuteration processes.

8. Conclusion

The torsion-rotational spectrum of mono-deuterated dimethyl ether (CH_3OCH_2D) was observed in the laboratory up to 1 THz. More than 2500 distinct lines were assigned to the symmetric and asymmetric conformers. The spectroscopic parameters given in Table 1 were determined for both species, and it allowed us to reproduce measurements with a standard deviation better than 105 kHz. They also have permitted transitions to be predicted up to 1.2 THz. Thanks to these frequency predictions, the symmetric and the asymmetric conformers of mono-deuterated dimethyl ether have been detected in the solar-type binary protostar IRAS 16293-2422. From an LTE modeling of these lines, together with lines from the main isotopomer, we concluded that dimethyl ether is highly deuterated in this source, with a D/H abundance ratio ~15%, as high as observed for methanol and formaldehyde, two species known to play important roles in the COMs formation history. Comparison of these species deuteration in hot cores might also contribute to a better understanding of the cold grain surface and warm gas-phase processes in the DME chemistry. A detailed and comparative study of the DME deuteration ratio in the two hot corinos of IRAS 16293, which are likely to present somewhat different evolutions due to their different masses, would provide crucial information on the chemical and physical history of the sources. With the high spatial resolution and sensitivity provided by the ALMA interferometer, such ambitious goals can be reached and will represent an important step towards understanding the history of solar-type systems like our own.

Acknowledgements. This work was supported by the CNES and the Action sur Projets de l'INSU, "Physique et Chimie du Milieu Interstellaire" and by the ANR-08-BLAN-0225 contracts.

[1] The CASSIS software was developed by IRAS-UPS/CNRS (http://cassis.irap.omp.eu/)

[2] The complete LTE formalism can be found on the CASSIS webpage.

References

Bacmann, A., Taquet, V., Faure, A., Kahane, C., & Ceccarelli, C. 2012, A&A, 541, L12
Blukis, U., Kasai, P. H., & Myers, R. J. 1963, J. Chem. Phys., 38, 2753
Bottinelli, S., Ceccarelli, C., Neri, R., et al. 2004, ApJ, 617, L69
Brouillet, N., Despois, D., Baudry, A., et al. 2013, A&A, 550, A46
Caux, E., Kahane, C., Castets, A., et al. 2011, A&A, 532, A23
Cazaux, S., Tielens, A., Ceccarelli, C., et al. 2003, ApJ, 593, L51
Ceccarelli, C., Castets, A., Caux, E., et al. 2000, A&A, 355, 1129
Ceccarelli, C., Caselli, P., Herbst, E., et al. 2007 (Tucson: University of Arizona Press), 951, 47
Coutens, A. 2012, Water deuteration in star-forming regions: Contribution of Herschel/HIFI spectroscopic data, Ph.D. Thesis, IRAP
Durig, J. R., Li, Y. S., & Groner, P. 1976, J. Molec. Spectrosc., 62, 159
Endres, C. P., Drouin, B. J., Pearson, J. C., et al. 2009, A&A, 504, 635
Endres, C. P., Müller, H. S. P., Lewen, F., et al. 2010, 65th OSU International Symposium on Molecular Spectroscopy
Gordy, W., & Cook, R. L. 1984, Microwave Molecular Spectroscopy (New York: Wiley)
Groner, P. 1997, J. Chem. Phys., 107, 4483
Groner, P. 2012, J. Mol. Spectrosc., 278, 52
Groner, P., Albert, S., Herbst, E., & De Lucia, F. C. 1998, ApJ, 500, 1059
Hartwig, H., & Dreizler, H. 1996, Z. Naturforsch, 51, 923
Herbst, E., & van Dishoeck, E. F. 2009, ARA&A, 47, 427
Ikeda, M., Ohishi, M., Nummelin, A., et al. 2001, ApJ, 560, 792
Jørgensen, J. K., Bourke, T. L., Nguyen Luong, Q., & Takakuwa, S. 2011, A&A, 534, A100
Linsky, J. L. 2003, Space Sci. Rev., 106, 49
Loinard, L., Castets, A., Ceccarelli, C., et al. 2000, A&A, 359, 1169
Loinard, L., Torres, R., Mioduszewski, A., & Rodrigez, L. 2008, Proc. IAU Symp., 218
Lovas, F. J., Lutz, H., & Dreizler, H. 1979, J. Phys. Chem. Ref. Data, 8, 1051
Motiyenko, R. A., Margulès, L., Alekseev, E. A., Guillemin, J. C., & Demaison, J. 2010, J. Molec. Spectrosc., 264, 94
Niide, Y., & Hayashi, M. 2003, J. Mol. Spectrosc., 148, 371
Parise, B., Ceccarelli, C., Tielens, A., et al. 2002, A&A, 393, L49
Peeters, Z., Rodgers, S. D., Charnley, S. B., et al. 2006, A&A, 445, 197
Pickett, H. M. 1991, J. Mol. Spectrosc., 148, 371
Pineda, J. E., Maury, A. J., Fuller, G. A., et al. 2012, A&A, 544, L7
Ratajczak, A., Taquet, V., Kahane, C., et al. 2011, A&A, 528, L13
Shtarev, A. B., Tian, F., Dolbier, W. R., Jr., & Smart, B. E. 1999, J. Am. Chem. Soc., 121, 7335
Snyder, L. E., Buhl, D., Schwartz, P. R., et al. 1974, ApJ, 191, L79
Watson, J. K. G. 1977, Vibrational Spectra and Structure (Amsterdam: Elsevier), 6, 1
Wooten, A. 1989, ApJ, 337, 858

Appendix A: Experimental frequencies

Table A.1. Experimental frequencies measured in laboratory up to 1 THz for the symmetric conformer.

σ^a	J'	K'_a	K'_c	J''	K''_a	K''_c	Frequency (MHz)	Uncertainty (MHz)	*o.-c.* (MHz)
...									
0	18	0	18	17	1	17	301 809.8746	0.030	−0.0063
1	18	0	18	17	1	17	301 809.8746	0.030	0.0129
1	15	2	14	14	1	13	302 890.5162	0.030	−0.0078
0	15	2	14	14	1	13	302 891.9278	0.030	−0.0016
1	18	1	18	17	0	17	305 194.2306	0.030	0.0723
0	18	1	18	17	0	17	305 194.2306	0.030	−0.0750
1	30	6	24	30	5	25	305 463.6078	0.030	0.0370
0	30	6	24	30	5	25	305 463.6078	0.030	−0.0574
0	29	6	23	29	5	24	308 587.0588	0.030	−0.1457
1	29	6	23	29	5	24	308 587.0588	0.030	0.1513
1	31	1	30	31	0	31	314 809.1205	0.030	0.0055
0	31	1	30	31	0	31	314 814.3153	0.030	0.0268
1	24	0	24	23	1	23	402 366.4331	0.030	0.0252
0	24	0	24	23	1	23	402 366.4331	0.030	−0.0384
0	24	1	24	23	0	23	402 947.7082	0.030	−0.0343
1	24	1	24	23	0	23	402 947.7082	0.030	0.0389
1	8	5	3	7	4	3	405 994.3663	0.030	0.0219
1	8	5	4	7	4	4	405 996.3966	0.030	−0.0080
0	8	5	4	7	4	3	405 998.2405	0.030	−0.0246
0	8	5	3	7	4	4	405 999.3242	0.030	0.0442
...									

Notes. Table A.1 appears in its entirety in electronic form at the CDS. [(a)] Symmetry number: 0(A), 1(E).

Table A.2. Experimental frequencies measured in laboratory up to 1 THz for the asymmetric conformer.

σ^a	J'	K'_a	K'_c	J''	K''_a	K''_c	Frequency (MHz)	Uncertainty (MHz)	*o.-c.* (MHz)
...									
0	18	1	17	17	2	16	308 574.0278	0.030	−0.0041
1	18	1	17	17	2	16	308 574.0278	0.030	−0.0119
0	20	2	18	19	3	17	309 332.3342	0.030	−0.1438
1	20	2	18	19	3	17	309 332.3342	0.030	0.1534
1	16	2	15	15	1	14	311 688.4409	0.030	0.0091
0	16	2	15	15	1	14	311 689.1054	0.030	0.0747
0	18	0	18	17	1	17	311 780.4497	0.030	−0.0262
1	18	0	18	17	1	17	311 780.4497	0.030	0.0278
0	18	1	18	17	0	17	313 464.4144	0.030	−0.0312
1	18	1	18	17	0	17	313 464.4144	0.030	0.0441
1	30	4	26	29	5	25	401 758.3919	0.030	−0.0360
0	30	4	26	29	5	25	401 759.3987	0.030	0.0572
1	14	3	11	13	2	12	402 976.5772	0.030	0.0066
0	14	3	11	13	2	12	402 978.7814	0.030	−0.0175
1	18	3	16	17	2	15	403 838.4379	0.030	−0.0282
0	18	3	16	17	2	15	403 839.6472	0.030	0.0224
0	23	1	22	22	2	21	404 504.7740	0.030	0.0929
1	23	1	22	22	2	21	404 504.7740	0.030	−0.1030
1	34	5	29	33	6	28	405 481.1146	0.030	0.0065
0	34	5	29	33	6	28	405 482.7182	0.030	0.0101
...									

Notes. Table A.2 appears in its entirety in electronic form at the CDS. [(a)] Symmetry number: 0(A), 1(E).

Appendix B: Predicted frequencies

Table B.1. Predicted transition frequencies of mono-deuterated DME in the ground-vibrational state for the symmetric conformer up to 1.2 THz.

σ^a	J'	K'_a	K'_c	J''	K''_a	K''_c	Frequency (MHz)	Uncertainty (MHz)	Spin weight	S	E' (cm^{-1})
...											
1	35	5	31	34	6	28	301 607.541	0.006	4	5.1343	395.904
0	35	5	31	34	6	28	301 608.196	0.006	4	5.1343	395.904
1	41	7	34	40	8	33	301 650.237	0.007	4	6.3063	555.166
0	41	7	34	40	8	33	301 651.158	0.008	4	6.3068	555.166
0	31	6	25	31	5	26	301 791.825	0.003	4	17.7370	327.325
1	31	6	25	31	5	26	301 791.952	0.003	4	17.7370	327.324
1	18	0	18	17	1	17	301 809.863	0.002	4	14.9891	97.540
0	18	0	18	17	1	17	301 809.882	0.002	4	14.9891	97.540
1	33	3	31	33	2	32	301 812.643	0.005	4	10.7481	336.889
0	33	3	31	33	2	32	301 815.237	0.006	4	10.7481	336.889
1	9	3	7	8	2	6	302 104.489	0.002	4	3.4020	35.287
0	9	3	7	8	2	6	302 107.944	0.003	4	3.4025	35.287
1	13	3	10	13	0	13	302 349.404	0.005	4	0.1877	62.456
0	13	3	10	13	0	13	302 355.581	0.006	4	0.1877	62.456
1	15	2	14	14	1	13	302 890.525	0.003	4	6.5291	73.991
0	15	2	14	14	1	13	302 891.930	0.003	4	6.5291	73.991
1	50	5	45	50	4	46	303 103.917	0.074	4	28.8858	784.222
0	50	5	45	50	4	46	303 104.619	0.074	4	28.8856	784.222
1	30	1	29	30	0	30	303 456.667	0.009	4	5.3792	272.161
0	30	1	29	30	0	30	303 461.701	0.009	4	5.3792	272.161
...											

Notes. Table B.1 appears in its entirety in electronic form at the CDS. [(a)] Symmetry number: 0(A), 1(E).

Table B.2. Predicted transition frequencies of mono-deuterated DME in the ground-vibrational state for the asymmetric conformer up to 1.2 THz.

σ^a	J'	K'_a	K'_c	J''	K''_a	K''_c	Frequency (MHz)	Uncertainty (MHz)	Spin weight	S	E' (cm^{-1})
...											
0	31	4	28	30	5	25	300 765.660	0.007	4	3.1152	315.519
1	31	4	28	30	5	25	300 765.839	0.007	4	3.1152	315.519
1	34	6	29	33	7	26	300 884.869	0.005	4	5.0260	393.250
0	34	6	29	33	7	26	300 885.555	0.005	4	5.0260	393.250
0	49	8	41	49	7	42	300 931.104	0.021	4	31.7689	801.251
1	49	8	41	49	7	42	300 934.607	0.018	4	31.7687	801.251
0	36	7	29	36	6	30	302 208.713	0.004	4	21.0996	447.329
1	36	7	29	36	6	30	302 210.202	0.004	4	21.0996	447.329
1	10	3	8	9	2	7	302 955.486	0.003	4	3.5150	41.122
0	10	3	8	9	2	7	302 957.701	0.004	4	3.5151	41.122
0	42	6	37	42	5	38	304 715.274	0.007	4	23.5168	581.371
1	42	6	37	42	5	38	304 716.691	0.006	4	23.5167	581.370
1	37	7	31	36	8	28	304 930.989	0.005	4	5.4586	469.848
0	37	7	31	36	8	28	304 931.783	0.005	4	5.4591	469.848
0	38	4	35	37	5	32	304 964.130	0.012	4	1.5197	463.341
1	38	4	35	37	5	32	304 964.965	0.012	4	1.5197	463.341
0	40	5	36	40	4	37	305 089.510	0.009	4	19.4294	520.912
1	40	5	36	40	4	37	305 089.932	0.009	4	19.4294	520.912
0	23	3	20	22	4	19	305 743.397	0.006	4	4.4529	177.930
1	23	3	20	22	4	19	305 743.761	0.006	4	4.4529	177.930
...											

Notes. Table B.2 appears in its entirety in electronic form at the CDS. [(a)] Symmetry number: 0(A), 1(E).